Turkish Journal of Electrical Engineering & Computer Sciences

http://journals.tubitak.gov.tr/elektrik/

Research Article

Turk J Elec Eng & Comp Sci
(2020) 28: 1355 – 1370

doi:10.3906/elk-1907-204

Low harmonic 12-pulse rectifier with a circulating current shaping circuit

Jingfang WANG[1], **Xuliang YAO**[1], **Qi GUAN**[1], **Changji DENG**[2], **Shiyan YANG**[3,*]
[1]No. 61 Building, College of Automation, Harbin Engineering University, Harbin, P.R. China
[2]XJ Power Co., Ltd, Xuchang, P.R. China
[3]School of Electrical Engineering and Automation, Harbin Institute of Technology, Harbin, P.R. China

Received: 27.07.2019 • **Accepted/Published Online:** 12.07.2020 • **Final Version:** 08.05.2020

Abstract: This paper proposes a four-star 12-pulse diode rectifier with a circulating current shaping circuit (CCSC) on the DC side to decrease the input current harmonics effectively. The type of circulating current that can eliminate the input current harmonics is analysed and its waveform parameters are derived. The effects of triangular circulating current on the harmonics of the input current are analysed, and the harmonic suppression mechanism of the triangular circulating current is revealed. This scheme has excellent harmonic suppression capability, and the capacity of CCSC is only 2.35% of output power of the 12-pulse rectifier. Thus, this scheme is cost effective for high power applications. The experimental results confirm the theoretical analysis and near sinusoidal input current is obtained.

Key words: 12-pulse diode rectifier, harmonic reduction, interphase reactor, circulating current

1. Introduction

The four-star 12-pulse diode rectifier, which possesses high reliability and low diode conduction losses, is often used in low-voltage and high-current applications like electrolysis, electroplates, heating coils, and DC arc furnaces [1–3]. Although the four-star 12-pulse diode rectifier can offset the 5th and 7th harmonics, the THD of input current is still high (about 15%), which cannot meet the requirement of IEEE-519 [4].

In high-power applications, various harmonic reduction approaches have been proposed. Installing passive power filters is a conventional method to reduce the input line current harmonics; however, they make the overall rectifier system bulky and expensive [5, 6]. Another way is to employ active power filters or hybrid power filters, but a complex control loop needs to be used and they involve high costs [7–12]. In previous studies [13, 14], to compensate the input current harmonics, three-phase PWM converters were connected in parallel with the 12-pulse rectifier. Although it can compensate for the input current harmonics effectively, the capacity of three-phase PWM converters is high and they are very complicated to control. For high power applications, increasing the number of pulses of the rectifier is an effective way to suppress harmonics [15–19]. In other previous work [15, 16], several cases of 24-pulse diode rectifiers with multiphase transformers were proposed. These cases provide almost constant output voltage and near sinusoidal input current. However, multiphase transformers require a large number of devices due to their complex structure. The double tapped interphase reactor (IPR) scheme is proposed and it has become a popular method for obtaining a 24-pulse rectifier with the simplest circuit structure [17, 18]. However, the conduction loss of the tapped IPR is high and it is not recommended for high-current applications. In Yang et al. [19], a low conduction losses pulse-multiplier circuit that consists of an IPR with additional secondary winding and an auxiliary single-phase rectifier is proposed. This scheme

*Correspondence: jingfangwang@hrbeu.edu.cn

can upgrade the conventional 12-pulse rectifier to a 24-pulse rectifier and has lower diode conduction losses. However, it has limited capability to suppress input current harmonics and the THD of input current remains high (approximately 7.5%). To reduce the harmonics of input current to a greater extent, a special DC–DC converter is connected in series with the 12-pulse rectifier to reduce the input current harmonics [20–22]. The harmonics can be well suppressed by this method and the input current THD is only about 3%. However, the two forced-commutated switches have a high current level and large conduction losses, which limit its applications in high-power situations. In Fukuda et al. [23], a 12-pulse diode rectifier with an auxiliary voltage source is presented; it adds an auxiliary voltage source to the secondary side of the IPR to form a specific circulating current. This method avoids the series connection between load and additional components. It has the advantages of simple circuit structure and easy control, but the performance of suppressing harmonics is greatly affected by the load parameters and the amplitude of the auxiliary voltage source. In Chen et al. [24], a 12-pulse rectifier with current injection is proposed to reduce the input current harmonics by connecting a flyback circuit to the added secondary windings of two IPRs. However, the kVA rating of the flyback circuit is still high (approximately 15.0% of the output power) and the practical harmonic suppression performance is not good. In addition, because of the nonisolation of input and output of this 12-pulse rectifier, it is not suitable for industrial application where the input and output voltages have large differences and both sides of the AC and DC need to be isolated.

In the present paper, a low harmonic four-star 12-pulse diode rectifier with a low power (2.35% of the output power) circulating current shaping circuit (CCSC) on the DC side is proposed (Figure 1). The CCSC generates a circulating current on the DC side of the rectifier to shape the input current into sinusoidal current. The CCSC is connected in parallel rather than in series with load and it avoids additional conduction losses. Compared with those methods using an auxiliary single-phase voltage converter to modulate the output current of the diode rectifier bridge [23], the proposed scheme using a CCSC shapes the output current of the 6-pulse rectifier (bridge) directly, and so the effects of load current variation on the ability to suppress harmonics are weakened.

2. Analysis of the injected current

Figure 1 shows the proposed four-star 12-pulse diode rectifier with a CCSC on the DC side.

In Figure 1, the proposed rectifier is nearly the same as the conventional four-star 12-pulse rectifier except for the second-stage interphase reactor. The conventional second-stage interphase reactor is replaced by the modified second-stage interphase reactor (MSIPR) and the CCSC. The additional secondary winding of the MSIPR is employed to install the CCSC. The CCSC extracts a triangular circulating current from this winding and shapes the output currents in the two double-star rectifiers. Then the sinusoidal input current is obtained according to the relation between the input currents and output currents of the two double-star rectifiers.

In Figure 1, we assume that the power supply of the proposed rectifier is an ideal three-phase voltage system and they meet

$$\begin{cases} u_a = U_1 sin(\omega t) \\ u_b = U_1 sin(\omega t - \dfrac{2\pi}{3}) \\ u_c = U_1 sin(\omega t + \dfrac{2\pi}{3}), \end{cases} \tag{1}$$

where U_1 is the amplitude of the input phase voltage.

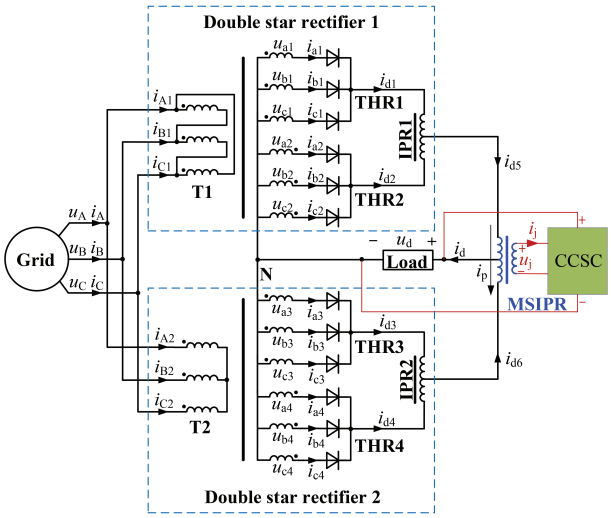

Figure 1. Four-star 12-pulse diode rectifier with a CCSC on the DC side.

The turns ratio between the primary windings and the secondary windings in double-star transformers (Y/Y/Y connection) is $k:1:1$.

In Figure 1, according to the magnetic motive force (MMF) relation and Kirchhoff's current law, the expression of the input currents can be obtained as

$$\begin{cases} i_A = \dfrac{1}{k}(i_{a1} - i_{a2} + i_{c2} - i_{c1} + \sqrt{3}i_{a3} - \sqrt{3}i_{a4}) \\ i_B = \dfrac{1}{k}(i_{b1} - i_{b2} + i_{a2} - i_{a1} + \sqrt{3}i_{b3} - \sqrt{3}i_{b4}) \\ i_C = \dfrac{1}{k}(i_{c1} - i_{c2} + i_{b2} - i_{b1} + \sqrt{3}i_{c3} - \sqrt{3}i_{c4}) \end{cases} \tag{2}$$

In Figure 1, the relation between the input and output currents of three-phase half-wave rectifiers (THR1, THR2, THR3, and THR4) is

$$\begin{cases} i_{a1} = i_{d1}S_{a1} = \dfrac{1}{2}i_{d5}S_{a1} \\ i_{a2} = i_{d2}S_{a2} = \dfrac{1}{2}i_{d5}S_{a2} \\ i_{a3} = i_{d3}S_{a3} = \dfrac{1}{2}i_{d6}S_{a3} \\ i_{a4} = i_{d4}S_{a4} = \dfrac{1}{2}i_{d6}S_{a4} \end{cases} \tag{3}$$

$$\begin{cases} i_{b1} = i_{d1}S_{b1} = \dfrac{1}{2}i_{d5}S_{b1} \\ i_{b2} = i_{d2}S_{b2} = \dfrac{1}{2}i_{d5}S_{b2} \\ i_{b3} = i_{d3}S_{b3} = \dfrac{1}{2}i_{d6}S_{b3} \\ i_{b4} = i_{d4}S_{b4} = \dfrac{1}{2}i_{d6}S_{b4} \end{cases} \tag{4}$$

$$\begin{cases} i_{c1} = i_{d1}S_{c1} = \dfrac{1}{2}i_{d5}S_{c1} \\ i_{c2} = i_{d2}S_{c2} = \dfrac{1}{2}i_{d5}S_{c2} \\ i_{c3} = i_{d3}S_{c3} = \dfrac{1}{2}i_{d6}S_{c3} \\ i_{c4} = i_{d4}S_{c4} = \dfrac{1}{2}i_{d6}S_{c4}, \end{cases} \tag{5}$$

where $S_{a1}, S_{b1}, S_{c1}, S_{a2}, S_{b2}, S_{c2}, S_{a3}, S_{b3}, S_{c3}, S_{a4}, S_{b4},$ and S_{c4} are the switching functions of diodes. S_{a1} is expressed as

$$S_{a1} = \begin{cases} 1 & \omega t \in [0, \dfrac{2\pi}{3}] \\ 0 & \omega t \in [\dfrac{2\pi}{3}, 2\pi] \end{cases} \tag{6}$$

The expressions for the other switching functions ($S_{b1}, S_{c1}, S_{a2}, S_{b2}, S_{c2}, S_{a3}, S_{b3}, S_{c3}, S_{a4}, S_{b4},$ and S_{c4}) can be easily obtained on the basis of the phase relation between the switching functions.

The circulating current generated by the CCSC is i_j and its reference direction is shown in Figure 1. Since the turns ratio between the primary windings and the secondary windings of the MSIPR is 1:m, the output currents of double-star rectifier 1 and double-star rectifier 2 can be expressed as

$$\begin{cases} i_{d5} = \dfrac{1}{2}i_d + mi_j \\ i_{d6} = \dfrac{1}{2}i_d - mi_j, \end{cases} \tag{7}$$

where i_d is the output current of the proposed 12-pulse diode rectifier. Substituting (3), (4), (5), (6), and (7) into (1), we can get the input line currents i_A, i_B, and i_C.

$$\begin{cases} i_A = \dfrac{1}{4}A_1 i_d + \dfrac{m}{2}A_2 i_j \\ i_B = \dfrac{1}{4}B_1 i_d + \dfrac{m}{2}B_2 i_j \\ i_C = \dfrac{1}{4}C_1 i_d + \dfrac{m}{2}C_2 i_j \end{cases} \tag{8}$$

where

$$\begin{cases} A_1 = (S_{a1} - S_{c1} + S_{c2} - S_{a2} + \sqrt{3}S_{a3} - \sqrt{3}S_{a4})/k \\ A_2 = (S_{a1} - S_{c1} + S_{c2} - S_{a2} + \sqrt{3}S_{a4} - \sqrt{3}S_{a3})/k \\ B_1 = (S_{b1} - S_{a1} + S_{a2} - S_{b2} + \sqrt{3}S_{b3} - \sqrt{3}S_{b4})/k \\ B_2 = (S_{b1} - S_{a1} + S_{a2} - S_{b2} + \sqrt{3}S_{b4} - \sqrt{3}S_{b3})/k \\ C_1 = (S_{c1} - S_{b1} + S_{b2} - S_{c2} + \sqrt{3}S_{c3} - \sqrt{3}S_{c4})/k \\ C_2 = (S_{c1} - S_{b1} + S_{b2} - S_{c2} + \sqrt{3}S_{c4} - \sqrt{3}S_{c3})/k \end{cases} \tag{9}$$

According to the three-phase rectification theory, when the input line current harmonic is zero, the input line currents are sinusoidal current and can be expressed as

$$\begin{cases} i_A = I_1 sin(\omega t) \\ i_B = I_1 sin(\omega t - \dfrac{2\pi}{3}) \\ i_C = I_1 sin(\omega t + \dfrac{2\pi}{3}) \end{cases} \tag{10}$$

Substituting (10) into (8) and solving (8), the required circulating current i_j can be obtained as

$$i_j = \frac{B_1 sin(\omega t) - A_1 sin(\omega t - \frac{2\pi}{3})}{2m[A_2 sin(\omega t - \frac{2\pi}{3}) - B_2 sin(\omega t)]} i_d \tag{11}$$

Under large inductance load conditions, the current i_d can be viewed as a constant I_d and the waveform of the required circulating current I_j is shown in Figure 2.

As shown in Figure 2, the shape of the required circulating current is very close to the standard triangular current; its frequency is 6 times that of the input line voltage and the amplitude is 0.5 m times that of the output current of the system. The triangular current with 300 Hz frequency and $0.5mI_d$ amplitude is an optional approximate method to simplify the calculation and its implementation, and the required circulating current i_j is expressed as

$$i_j = \begin{cases} \dfrac{6I_d}{m\pi}(\omega t - \dfrac{p\pi}{3}) - \dfrac{I_d}{2m} & \omega t \in [\dfrac{p\pi}{3}, \dfrac{p\pi}{3} + \dfrac{\pi}{6}] \\ -\dfrac{6I_d}{m\pi}(\omega t - \dfrac{p\pi}{3}) + \dfrac{3I_d}{2m} & \omega t \in [\dfrac{p\pi}{3} + \dfrac{\pi}{6}, \dfrac{\pi(p+1)}{3}], \end{cases} \tag{12}$$

where $p = 0, 1, 2, 3, 4, 5$

Substituting (12) into (8), the Fourier expression of the input current is

$$\begin{cases} i_A = \sum_{n=1}^{\infty} B_n sin(n\omega t) \\ i_B = \sum_{n=1}^{\infty} B_n sin[n(\omega t - \frac{2\pi}{3})] \\ i_C = \sum_{n=1}^{\infty} B_n sin[n(\omega t + \frac{2\pi}{3})], \end{cases} \tag{13}$$

where

$$\begin{aligned} B_n = & \frac{-6I_d sin(\frac{n\pi}{2})cos(\frac{n\pi}{6}) - 2\sqrt{3}I_d sin(\frac{n\pi}{2})cos(\frac{n\pi}{3})}{k\pi^2 n^2} + \frac{4I_d sin(\frac{n\pi}{2})cos(\frac{n\pi}{3}) - 2I_d sin(\frac{n\pi}{2})cos(\frac{n\pi}{2})}{k\pi^2 n^2} \\ & + \frac{4\sqrt{3}I_d sin(\frac{n\pi}{2})cos(\frac{n\pi}{6}) + 2(2-\sqrt{3})I_d sin(\frac{n\pi}{2})}{k\pi^2 n^2} \end{aligned} \tag{14}$$

From (14), it is noted that the $n = 12h \pm 1$ order harmonics are suppressed effectively. The THD of the input currents is reduced from 15.2% to 1.06% and near sinusoidal input currents are obtained (see Figure 3).

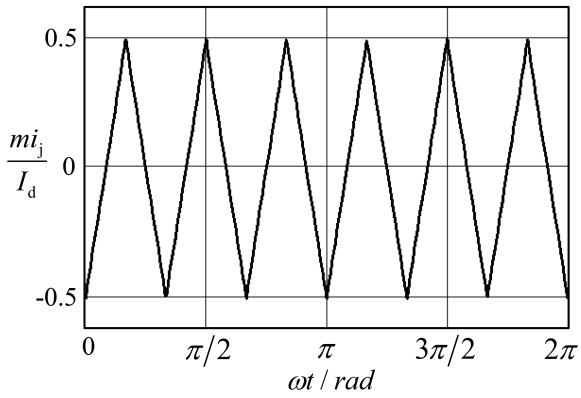

Figure 2. Circulating current i_j.

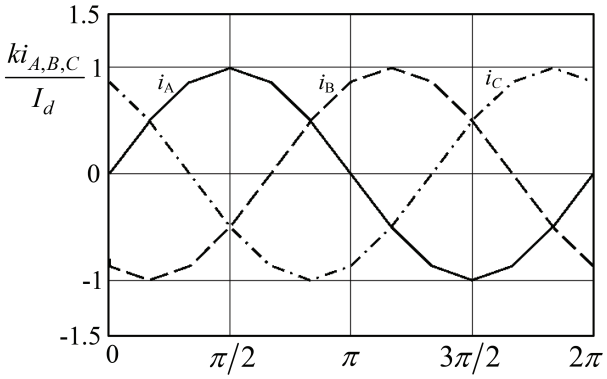

Figure 3. Input line current i_A, i_B, and i_C with current injection.

3. Harmonic suppression mechanism of the circulating current

In this section, the effect of the circulating current on the harmonics in the input currents is analysed and the harmonic suppression mechanism of the circulating current to the input current harmonic is presented.

When the circulating current i_j is generated by the CCSC on the DC side, the input current i_A can be obtained as

$$i_A = i_{A0} + i_{Apt} = \frac{1}{4}A_1 I_d + \frac{m}{2}A_2 i_j \tag{15}$$

In (15), the input line current i_A includes the current i_{A0} and the current i_{Apt}. The current i_{A0} refers to the input current of the conventional four-star 12-pulse diode rectifier, while the current i_{Apt} is the

corresponding embodiment of the circulating current i_j in the input current. In the conventional four-star 12-pulse diode rectifier, the expression of the input current i_{A0} is

$$i_{A0} = \frac{1}{4} A_1 I_d \tag{16}$$

Its Fourier expression is

$$i_{A0} = \frac{3I_d}{k\pi} sin(\omega t) + \sum_{\substack{n=12\pm1 \\ h=1,2,3...}}^{\infty} \frac{3I_d}{k\pi n} sin(n\omega t) \tag{17}$$

The expression of the current i_{Apt} is

$$i_{Apt} = \frac{m}{2} A_2 I_j \tag{18}$$

Substituting (9) and (12) into (18) and combing and performing Fourier series decomposition, the Fourier series expression of the current i_{Apt} is

$$i_{Apt} = \frac{3I_d}{\pi k}[(K-1)sin(\omega t) - \frac{1}{n} \sum_{\substack{n=12h-1 \\ h=1,2,3...}}^{\infty} (\frac{K}{n}+1) sin(n\omega t)] + \frac{3I_d}{\pi nk} \sum_{\substack{n=12h+1 \\ h=1,2,3...}}^{\infty} (\frac{K}{n}-1) sin(n\omega t), \tag{19}$$

where $K = \frac{12(2-\sqrt{3})}{\pi} = 1.023$.

In (19), the current i_{Apt} consists of three parts: the fundamental component, the $n = 12h-1$ order harmonic component, and the $n = 12h+1$ order harmonic component. Comparing with the expression (17), we can draw the following conclusions:

(1) The amplitude of the fundamental component in the current i_{Apt} is 0.023 times that of the input current of the conventional four-star 12-pulse rectifier. Thus, the current i_{Apt} increases the amplitude of the fundamental component of the input line current i_{A0} by 1.023 times, which helps increase the power factor;

(2) The amplitude of the $n = 12h-1$ order harmonic components in the current i_{Apt} is $1.023/n+1$ times that of the input current i_{A0}, but the signs are opposite. The i_{Apt} changes the polarity of this order harmonic component of the input current and reduces its amplitude by a factor of $1.023/n$;

(3) The amplitude of the $n = 12h+1$ order harmonic components in i_{Apt} is $1.023/n-1$ times that of the input current of the conventional four-star 12-pulse rectifier. It reduces the same order harmonic component to $1.023/n$ times that of the input current i_{A0}.

Based on the above analysis, the fundamental component of the input current increases slightly because of the circulating current i_j, the $n = 12h \pm 1$ order harmonics contained in the input current decrease significantly, and the harmonic suppression efficiency increases with the order of harmonics. These findings indicate the circulating current could considerably reduce the high and low order harmonics in the input current simultaneously.

4. CCSC for the circulating current generation

The input characteristics CCSC should be analysed first to generate triangular current by the CCSC, and the parameter design of CCSC is presented.

4.1. Input characteristics of the CCSC

Since the CCSC is installed in the secondary winding of the MSIPR, it has the same input characteristics as the secondary winding of the MSIPR. According to the three-phase rectification theory, the expression of the voltage u_j across the secondary winding of the MSIPR, which is also the input voltage of the CCSC, is

$$u_j = mu_p = \begin{cases} \sqrt{3}mU_2 sin(\frac{\pi}{12})sin(x - \frac{\pi p}{3} - \frac{\pi}{12}) & \omega t \in [\frac{p\pi}{3}, \frac{p\pi}{3} + \frac{\pi}{6}] \\ -\sqrt{3}mU_2 sin(\frac{\pi}{12})sin(x - \frac{\pi p}{3} - \frac{\pi}{4}) & \omega t \in [\frac{p\pi}{3} + \frac{\pi}{6}, \frac{\pi(p+1)}{3}], \end{cases} \tag{20}$$

where $p = 0, 1, 2, 3, 4, 5$; U_2 is the amplitude of the output voltage of the double-star transformer and meets

$$U_2 = \sqrt{3}U_1/k \tag{21}$$

The RMS of the voltage U_J can be calculated as

$$U_j = m\sqrt{\frac{1}{2\pi}\int_0^{2\pi} {u_j}^2 d\omega t} = 0.0814mU_d \tag{22}$$

Combined with (12), Figure 4 shows the circulating current i_j and the input voltage u_j of the CCSC.

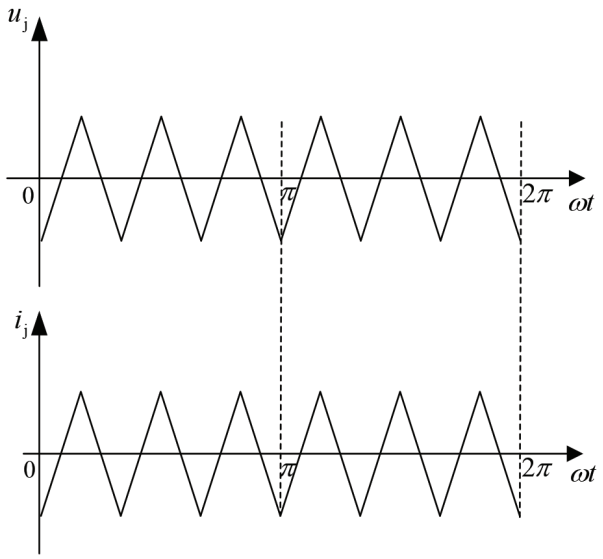

Figure 4. Input voltage u_j and circulating current i_j.

Figure 4 shows the symmetrical triangular waves, whose frequency is six times that of the input line voltage, and the phases of which are the same. The input characteristics of the CCSC are purely resistive and it should operate in a condition to unit power factor. According to Equations (20) and (22), the capacity of the CCSC can be calculated as (23)

$$P_{pcsc} = \int_0^{2\pi} u_j i_j d\omega t = 2.35\% U_d I_d = 2.35\% P_o \tag{23}$$

From the equation above, the capacity of the CCSC is only 2.35% that of the rectifier system. This method is cost effective for high power industrial applications.

Based on the analysis above, Figure 5 shows the schematic of the CCSC. The output of the CCSC is connected in parallel with the output of the 12-pulse rectifier, and so its output voltage is clamped by the output voltage of the proposed system, and only one current control loop is needed. In Figure 5, the reference signal of the circulating current is obtained by multiplying the average value of output current by the synchronous unit triangular wave signal (phase and frequency are the same as (12)). When the load changes, the reference signal changes accordingly, and the CCSC is adjusted to generate a corresponding triangular circulating current to ensure the CCSC has good harmonic suppression ability.

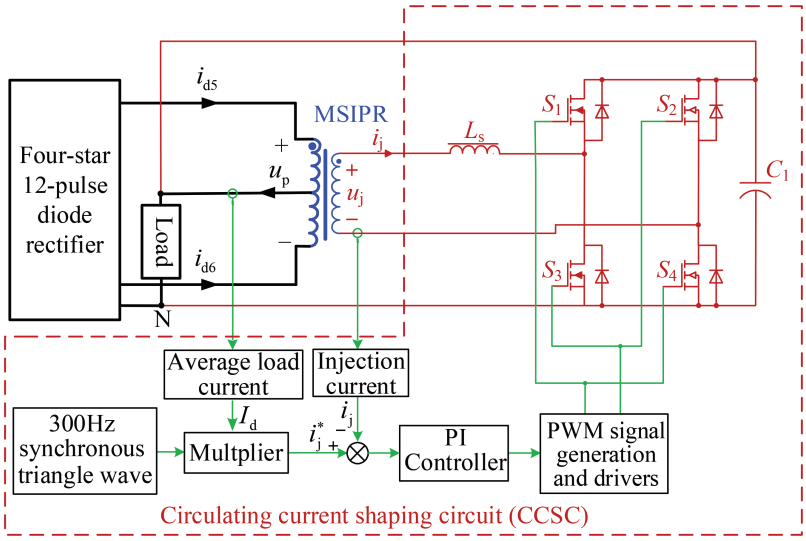

Figure 5. Schematic diagram of the CCSC.

4.2. Main circuit design for the CCSC

The previous analysis shows that the harmonic of the input current is effectively suppressed when the CCSC produces a triangular circulating current that satisfies Equation (12) on the DC side of the rectifier. Therefore, a reasonable design of the CCSC to generate the required circulating current is the key to suppress the harmonic of the input current effectively. In Figure 5, the main circuit parameters of the CCSC mainly include input inductance L_s and output voltage spike suppression capacitor C_1.

Voltage spike suppression capacitor C_1 is mainly used to suppress voltage spikes caused by wires and dispersed inductors in the CCSC. This capacitor can select appropriate capacitance values according to the length of the wire. Normally, capacitance ranges from a few μF to a few tens of μF.

The control of the input current to the CCSC refers to the control of the current in the input inductor L_s. L_s should be selected according to the input current ripple requirements and tracking speed to achieve good current control. In Figure 5, the CCSC scheme adopts bipolar modulation mode. A switching period T is divided into two parts. During the interval $T - T_s$, S1 and S4 are switched on, $u_j = U_d$, and the current on L_s satisfies

$$\Delta i_{j1} = (u_j - U_d)T_s/L_s, \tag{24}$$

where U_d is average value of load voltage.

During the interval $T_s - T$, S_2 and S_3 are switched on, $u_j = -U_d$, and the current on L_s satisfies

$$\Delta i_{j2} = (U_d + u_j)(T - T_s)/L_s \tag{25}$$

During the circuit operation, the ripple of the current through the inductor L_s should be limited to reduce the influence of high harmonics on the rectifier system, that is, the amplitude of the current ripple in each switching period should be less than or equal to the maximum ripple peak Δi_{jm} allowed by the current. For bipolar modulation, the worst case of ripple amplitude occurs at the peak of the input voltage; hence, the current ripple only needs to be satisfied at this time

$$\begin{cases} |\Delta i_{j1}| = (U_d - U_{jm})T_s/L_s \le \Delta i_{jm} \\ |\Delta i_{j2}| = (U_d + U_{jm})(T - T_s)/L_s \le \Delta i_{jm}, \end{cases} \tag{26}$$

where U_{jm} is the peak value of the input value u_j of the CCSC.

As switching frequency is very high, at the peak of the input voltage, $|\Delta i_{j1}| \approx |\Delta i_{j2}|$.

According to Equation (26), L_s is satisfied when the ripple requirements meet

$$L_s \ge \frac{({U_d}^2 - {U_{jm}}^2)T}{2\Delta i_{jm} U_d} \tag{27}$$

Another important selection principle of inductor Ls is the current tracking speed. Given that the circuit proposed in the present paper needs to control the triangular current to 6 times the power grid frequency, it only needs to make the current change rate greater than or equal to the current slope of the required triangular current within a switching period near the zero crossing of the input voltage, that is

$$\left| \frac{|\Delta i_{j1}| - |\Delta i_{j2}|}{T} \right| \ge \frac{6\omega I_m}{\pi} = \frac{6\omega I_d}{\pi m} \tag{28}$$

Substituting (24) and (25) into (28),

$$L_s \le \left| \frac{U_d(T - 2T_s)}{T} \right| \frac{m\pi}{6\omega I_d} \tag{29}$$

To meet the tracking speed, $T_s = T$ can be applied, and L_s in Equation (29) can be expressed as follows:

$$L_s \le \frac{m\pi U_d}{6\omega I_d} \tag{30}$$

In summary, the value of the input inductance Ls of the PWM rectifier should meet

$$\frac{({U_d}^2 - {U_{jm}}^2)T}{2\Delta i_{jm} U_d} \le L_s \le \frac{m\pi U_d}{6\omega I_d} \tag{31}$$

5. Experimental results

A 2.5-kW experimental prototype is developed to verify the theoretical analysis above. The main parameters are shown in Table 1.

Table . Main parameters of the prototype.

Name	Parameters
Three-phase input line voltage RMS	380 V
Double-star transformer turns ratio (Y/Y/Y)	4.7:1:1
Double-star transformer turns ratio (△/Y/Y)	8.2:1:1
Load filtering inductance	4.8 mH
Rated output power	2.5 kW
Turns ratio of the MSIPR	1:3.5
Input filtering inductance of CCSC	1.8 mH
Switching frequency of CCSC	40 kHz

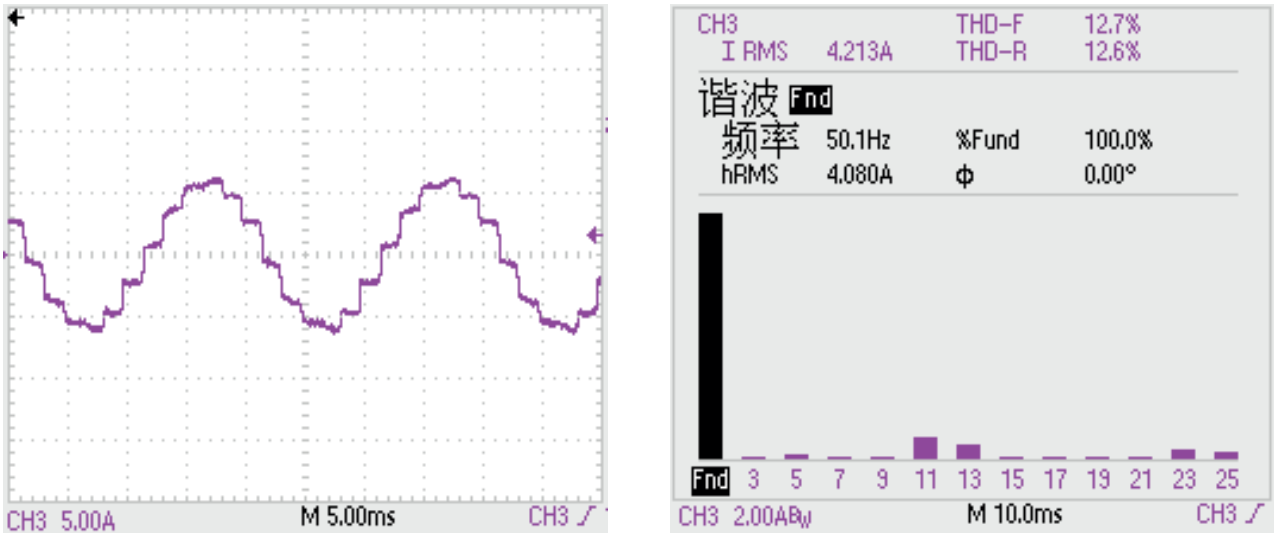

(a) Input line current i_A

(b) Spectrum of i_A

Figure 6. Measured waveforms without the CCSC.

Under the rated conditions shown in Table 1, Figures 6 and 7 show the experimental waveforms without and with the CCSC, respectively. If the CCSC is not in operation, there will not be any circulating current on the DC side. In that occasion, the proposed rectifier performs as a conventional four-star 12-pulse rectifier. The input current and its spectrum are shown in Figure 6.

In Figure 6, the input current is 12-step current and the THD of the input current is 12.7%, which is 15.2% less than the theoretical value because of the leakage inductances of the transformer.

When the CCSC works normally, it generates the required circulating current and the proposed rectifier draws near sinusoidal input current with less than 5% THD. Figure 7 shows experimental waveforms when the CCSC works normally.

Figures 7a and 7b show the circulating current generated by the CCSC and the load current, respectively. The circulating current is a symmetrical triangular current with 300 Hz frequency and 7 A amplitude. The amplitude of the current is about 1/7 of the load current (49.3 A), which is basically consistent with the above theoretical analysis. Figures 7c and 7d show the currents i_{d5} and i_{d6}; they are critical continuous triangular

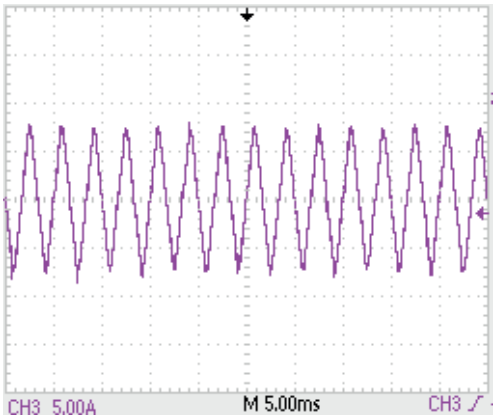

(a) Circulating current i_j

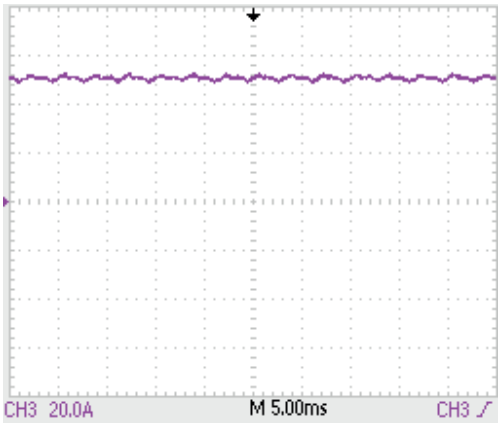

(b) Output current ofthe proposed 12- pulse rectifier

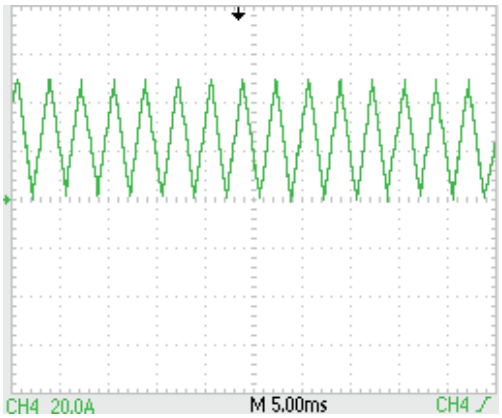

(c) Double-star rectifier 1 output current i_{d5}

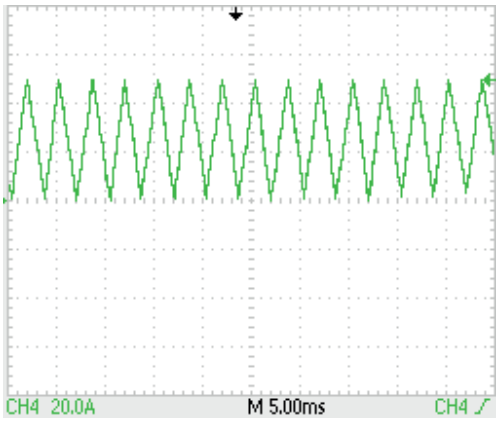

(d) Double-star rectifier 2 output current i_{d6}

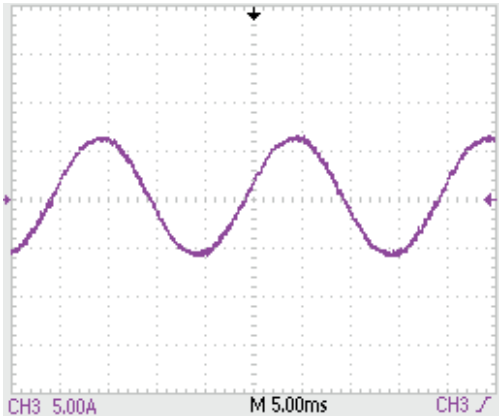

(e) Input current i_A

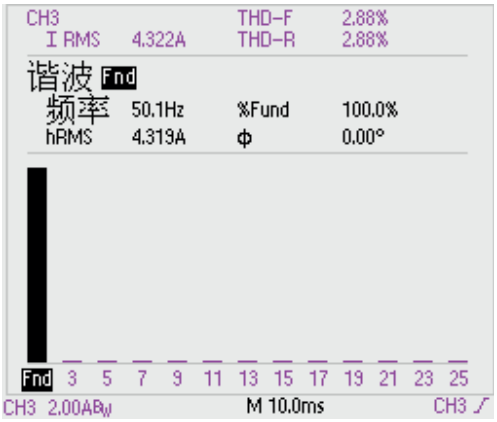

(f) Spectrum of i_A

Figure 7. Experimental waveforms with the CCSC.

current with a frequency of 300 Hz and an amplitude of 49.3 A and they coincide with the theoretical analysis. Figures 7e and 7f show the input current and its spectrum. Comparing with Figures 6a and 6b, it is noted that the circulating current generated by the CCSC can effectively reduce input current harmonics. The THD of

input current drops from 11.7% to 2.88%, and the 11th, 13th, 23th, and 25th harmonics in the input current are reduced effectively.

To compare with the proposed method in this paper, Figure 8 shows the input current waveform and spectrum of the 12-pulse rectifier as the auxiliary voltage supply (AVS) scheme mentioned in Fukuda et al. [23] is applied.

As shown in Figure 8, the THD of the input current is reduced to 4.1% after the adoption of AVS and the harmonic of the input current is suppressed effectively. However, the THD of the input current is slightly higher than that of the input current (2.9%) when the CCSC scheme is applied because the modulation of the AVS on the output current of the rectifier bridge is indirect, and the harmonic suppression effect is slightly worse than that of the CCSC scheme.

Figure 9 shows the relationship between the input line current THD and the load current when the AVS scheme in Fukuda et al. [23] and the CCSC scheme proposed in the present paper perform under different load conditions (10 A, 18 A, 30 A, 43 A, and 49.3 A).

In Figure 9, the CCSC scheme has stronger harmonic suppression ability and lower input line current THD than the AVS scheme. When the load current changes from 18 A to 49.3 A, the THD variation range of the input current reaches as high as 3% when the AVS scheme is applied. However, the THD variation range of the input current is only 1.7% when the CCSC scheme proposed in the present paper is adopted, indicating that the method proposed herein has a strong ability to adapt to variation in the load current.

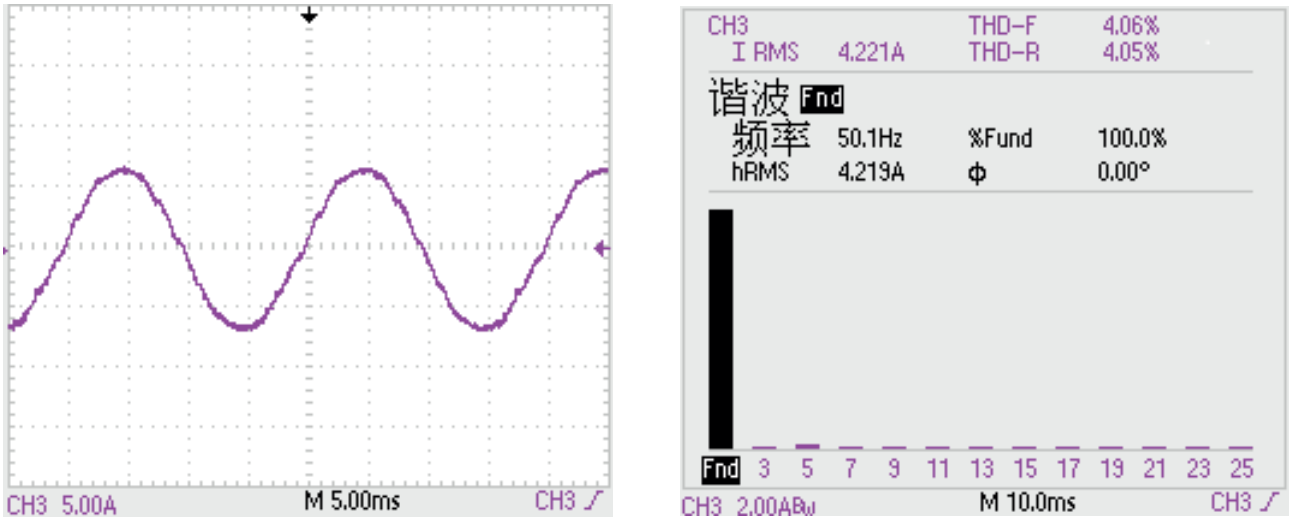

(a) Waveform of input current

(b) Spectrum of input current

Figure 8. Input current and its spectrum when the AVS scheme is applied.

Figure 10 shows the PF of a conventional 12-pulse rectifier and a 12-pulse rectifier with the CCSC on the DC side under different load conditions.

Figure 10 shows that after installing the CCSC on the DC side of the rectifier, the PF of the system is increased by approximately 1%, indicating that the PF of the system can be slightly improved by using a CCSC.

Figure 11 shows the efficiency of the conventional 12-pulse rectifier and 12-pulse rectifier with the CCSC on the DC side under different load conditions.

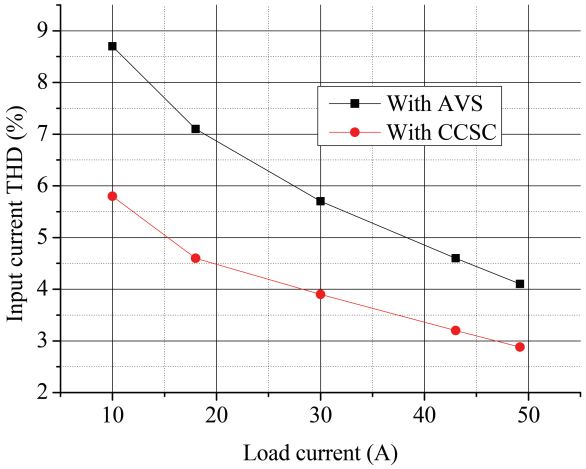

Figure 9. Relation between THD values and load current.

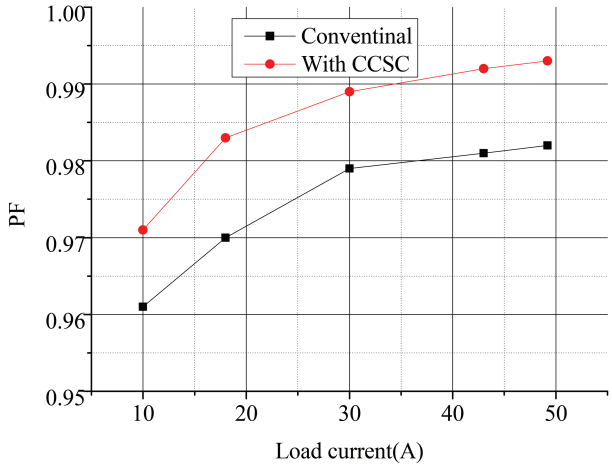

Figure 10. Relation between PF and load current.

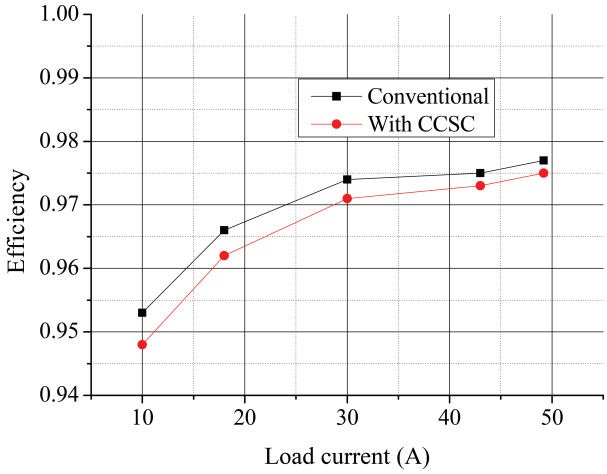

Figure 11. Relation between efficiency and load current.

As shown in Figure 11, the efficiency of the rectifier system changes slightly before and after the adoption of the CCSC. The reason is that the CCSC feeds the extracted harmonic energy back to the load, thereby avoiding the waste of harmonic energy so that the 12-pulse rectifier with the CCSC on the DC side can also achieve high efficiency.

6. Conclusions

This paper proposes a CCSC scheme to reduce the input current harmonics of a four-star 12-pulse diode rectifier effectively. The low power CCSC is connected with the additional winding of the MSIPR, and it generate a specific triangular circulating current to modulate the output current of two double-star rectifiers first, which in turn shape a near sinusoidal input line current with less than 5% THD. The input characteristics of the CCSC are analysed and the input design method of the CCSC is presented. The theoretical and experimental results show that when the input line harmonics are reduced significantly, the CCSC operates in a unit power factor condition, and its input characteristics are purely resistive. As the capacity of the CCSC is only 2.35% of

the output power of the proposed rectifier, this method is cost effective and suitable for high-power industrial applications.

Acknowledgement

This research is supported by the Fundamental Research Funds for the Central Universities (HEUCFJ180403, 3072019CF0403).

References

[1] Solanki J, Fröhleke N, Böcker J, Averberg A, Wallmeler P. High-current variable voltage rectifiers: state of the art topologies. IET Power Electronics 2015; 8 (6):1068-1080. doi: 10.1049/iet-pel.2014.0533

[2] Singh B, Gairola S, Singh BN, Chandra A, Al-Haddad K. Multipulse AC–DC converters for improving power quality: a review. IEEE Transactions on Power Electronics 2008; 23 (1): 260-281. doi: 10.1109/TPEL.2007.911880

[3] Li S, Luo L, She S, Liu L, Shi X. Synthetic energy-saving interruptible 6-pulse rectifier system for manganese electrolyzation. Electric Power Automation Equipment 2016; 36 (7): 131-137. doi: 10.16081/j.issn.1006-6047.2016.07.020

[4] IEEE guide for recommended control and reactive compensation of static power converters, IEEE Std. 519, 1992.

[5] Li X, Xu W, Ding T. Damped high passive filter - a new filtering scheme for multipulse rectifier systems. IEEE Transactions on Power Delivery 2017; 32 (1): 117-124. doi: 10.1109/TPWRD.2016.2541621

[6] Singh S, Singh B. Power quality improvement using optimized Passive Filter for 12-pulse rectifier-chopper in LCI fed synchronous motor drives. In: 2011 World Congress on Information and Communication Technologies; Mumbai, India; 2011. pp. 1104-1111.

[7] Hamad MS, Masoud M I, Ahmed KH, Williams BW. A shunt active power filter for a medium-voltage 12-pulse current source converter using open loop control compensation. IEEE Transactions Industrial Electronics 2014; 61 (11): 5840-5850. doi: 10.1109/TIE.2014.2311388

[8] Terciyanli A, Ermis M, Cadirci I. A selective harmonic amplification method for reduction of kVA rating of current source converters in shunt active power filters. IEEE Transactions on Power Delivery 2011; 26 (1): 65-78. doi: 10.1109/TPWRD.2010.2078838

[9] Patil SS, Metri RA, Shinde OK. Shunt active power filter for MV 12-pulse rectifier using PI with SMC controller. In: 2017 International Conference on Circuit, Power and Computing Technologies (ICCPCT); Kollam, India; 2017. pp. 1-6.

[10] Leroux AD, Mouton HT, Akagi H. DFT-based repetitive control of a series active filter integrated with a 12-pulse diode rectifier. In: 2007 IEEE Power Electronics Specialists Conference; Orlando, FL, USA; 2007. pp. 2997-3002.

[11] Zhang Z, Zeng L, Zhang G, Rao R, Yi M. Control method of hybrid inductive filtering system based on energy model. Electric Power Automation Equipment 2018; 38 (10): 101-107. doi: 10.16081/j.issn.1006-6047.2018.10.016

[12] Solanki J, Fröhleke N, Böcker J. Implementation of hybrid filter for 12-pulse thyristor rectifier supplying high-current variable voltage DC load. IEEE Transactions on Industrial Electronics 2015; 62 (8): 4691-4701. doi: 10.1109/TIE.2015.2393833

[13] Izadinia R, Karshenas HR. Current shaping in a hybrid 12-pulse rectifier using a Vienna rectifier. IEEE Transactions on Power Electronics 2018; 33 (2): 1135-1142. doi: 10.1109/TIE.2015.2393833

[14] Hou C, Tsai CH. Design of an auxiliary converter for 12-pulse diode rectifiers. In: 2017 IEEE 3rd International Future Energy Electronics Conference and ECCE Asia (IFEEC 2017 - ECCE Asia); Kaohsiung, Taiwan; 2017. pp. 231-235.

[15] Monroy AO, Le-Huy H, Lavoie C. Modeling and simulation of a 24-pulse transformer rectifier unit for more electric aircraft power system. In: 2012 Electrical Systems for Aircraft, Railway and Ship Propulsion; Bologna, Italy; 2012. pp. 10-15.

[16] Joseph A, Wang J, Pan Z, Chen L, Peng FZ. A 24-pulse rectifier cascaded multilevel inverter with minimum number of transformer windings. In: Fortieth IAS Annual Meeting; Kowloon, Hong Kong, China; 2005. pp. 115-120.

[17] Pan Q, Ma W, Liu D, Zhao Z, Meng J. A new critical formula and mathematical model of double-tap interphase reactor in a six-phase tap-changer diode rectifier. IEEE Transactions on Industrial Electronics 2007, 54 (1): 479-485. doi: 10.1109/TIE.2006.888800

[18] Yang S, Meng F, Yang W. Optimum design of inter-phase reactor with double tap-changer applied to multi-pulse diode rectifier. IEEE Transactions on Industrial Electronics 2010; 57 (9): 3022-3029. doi: 10.1109/TIE.2009.2038393

[19] Yang S, Wang J, Yang W. A novel 24-pulse diode rectifier with an auxiliary single-phase full-wave rectifier at DC side. IEEE Transactions on Power Electronics 2017; 32 (3): 1885-1893. doi: 10.1109/TPEL.2016.2560200

[20] Villablanca ME, Nadal JI, Bravo MA. A 12-pulse AC-DC rectifier with high-quality input/output waveforms. IEEE Transactions on Power Electronics 2007; 22 (5): 1875-1881. doi: 10.1109/TPEL.2007.904185

[21] Swamy MM. An electronically isolated 12-pulse autotransformer rectification scheme to improve input power factor and lower harmonic distortion in variable-frequency drives. IEEE Transactions on Industry Applications 2015; 51 (5): 3986-3994. doi: 10.1109/TIA.2015.2417123

[22] De Oliveira Costa Neto A, Soares AL, De Lima GB, Rodrigues DB, Coelho EAA et al. Optimized 12-pulse rectifier with generalized delta connection autotransformer and isolated SEPIC converters for sinusoidal input line current imposition. IEEE Transactions on Power Electronics 2019; 34 (4): 3204-3213. doi: 10.1109/TPEL.2018.2850280

[23] Fukuda S, Ohta M, Iwaji Y. An auxiliary-supply-assisted harmonic reduction scheme for 12-pulse diode rectifiers. IEEE Transactions on Power Electronics 2008; 23 (3): 1270-1277. doi: 10.1109/TPEL.2008.921165

[24] Chen Q, Mao L, Ren X, Ruan X, Jiang L. Research of the current-injection-based P-type 12-pulse ATRU. In: IEEE 7th International Power Electronics and Motion Control Conference; Harbin, China; 2012. pp. 41-46.